



**HAL**  
open science

# Comparative Study on the Interest in Non-Uniform Rational B-Splines Representation versus Polynomial Surface Description in a Freeform Three-Mirror Anastigmat

Clément Freslier, Guillaume Druart, Alice Fontbonne, Thierry Lépine, Christophe Buisset, Tibor Agocs, Arnaud Heliere, Fanny Keller, Jean-Baptiste Volatier, Stéphane Beaussier, et al.

► **To cite this version:**

Clément Freslier, Guillaume Druart, Alice Fontbonne, Thierry Lépine, Christophe Buisset, et al.. Comparative Study on the Interest in Non-Uniform Rational B-Splines Representation versus Polynomial Surface Description in a Freeform Three-Mirror Anastigmat. *Photonics*, 2024, 11 (9), pp.875. 10.3390/photonics11090875 . hal-04714681

**HAL Id: hal-04714681**

**<https://hal.science/hal-04714681v1>**

Submitted on 30 Sep 2024

**HAL** is a multi-disciplinary open access archive for the deposit and dissemination of scientific research documents, whether they are published or not. The documents may come from teaching and research institutions in France or abroad, or from public or private research centers.


L'archive ouverte pluridisciplinaire **HAL**, est destinée au dépôt et à la diffusion de documents scientifiques de niveau recherche, publiés ou non, émanant des établissements d'enseignement et de recherche français ou étrangers, des laboratoires publics ou privés.



Distributed under a Creative Commons Attribution 4.0 International License

## Article

# Comparative Study on the Interest in Non-Uniform Rational B-Splines Representation versus Polynomial Surface Description in a Freeform Three-Mirror Anastigmat

Clément Freslier <sup>1,\*</sup>, Guillaume Druart <sup>1</sup>, Alice Fontbonne <sup>1</sup>, Thierry Lépine <sup>2</sup>, Christophe Buisset <sup>3</sup>, Tibor Agocs <sup>3</sup>, Arnaud Heliere <sup>3</sup>, Fanny Keller <sup>3</sup>, Jean-Baptiste Volatier <sup>4</sup>, Stéphane Beaussier <sup>5</sup> and Paul Jouglà <sup>6</sup>

<sup>1</sup> DOTA, ONERA, Université Paris-Saclay, 91120 Palaiseau, France; guillaume.druart@onera.fr (G.D.); alice.fontbonne@onera.fr (A.F.)

<sup>2</sup> Laboratoire Hubert Curien UMR 5516n, CNRS, Institut d'Optique Graduate School, Université Jean Monnet Saint-Etienne, F-42023 Saint-Etienne, France; thierry.lepine@institutoptique.fr

<sup>3</sup> European Space Agency, ESTEC, Keperplaan 1, 2202 AG Noordwijk, The Netherlands; christophe.buisset@esa.int (C.B.); tiber.agocs@esa.int (T.A.); arnaud.heliere@esa.int (A.H.); fanny.kellet@esa.int (F.K.)

<sup>4</sup> Constellr, Heinrich-von-Stephan Straße, 5c, 79100 Freiburg, Germany; jbv@pm.me

<sup>5</sup> Valley Optics, Molengraaffsingel 12, 2629 JD Delft, The Netherlands; stefanjonbeaussier@protonmail.com

<sup>6</sup> Airbus Defence and Space, Rue des Cosmonautes, 31, 31402 Toulouse, France; paul.jouglà@airbus.com

\* Correspondence: clement.freslier@onera.fr

**Abstract:** Novel freeform optical design methods can be classified in two categories, depending on whether they focus on the generation of a starting point or the development of new optimization tools. In this paper, we design a freeform three-mirror anastigmat (TMA) and compare different surface representations using either a differential ray tracer as a new optimization tool or a commercial ray tracer (ANSYS-ZEMAX OpticStudio). For differential ray tracing, we used FORMIDABLE (Freeform Optics Raytracer with Manufacturable Imaging Design cApaBiLitiEs), an optical design library with differential ray tracing and Non-Uniform Rational B-Splines (NURBS) optimization capabilities, available under the European Software Community License (ESCL). NURBS allow a freeform surface to be represented without needing any prior knowledge of the surface, such as the polynomial degree in polynomial descriptions. OpticStudio and other commercial optical design software are designed to optimize polynomial surfaces but are not well-suited to optimize NURBS surfaces, requiring a custom optical design library. In order to demonstrate the interest in using NURBS representation, we designed and independently optimized two freeform telescopes over different iteration cycles; with NURBS using FORMIDABLE or with XY polynomials using OpticStudio. We then compared the resulting systems using their root mean square field maps to assess the optimization quality of each surface representation. We also provided a full-system comparison, including mirror freeform departures. This study shows that NURBS can be a relevant alternative to XY polynomials for the freeform optimization of reflective three-mirror telescopes as it achieves more a uniform imaging quality in the field of view.

**Keywords:** optimization; freeform; NURBS; differential ray tracer; XY polynomials; TMA



**Citation:** Freslier, C.; Druart, G.; Fontbonne, A.; Lépine, T.; Buisset, C.; Agocs, T.; Heliere, A.; Keller, F.; Volatier, J.-B.; Beaussier, S.; et al. Comparative Study on the Interest in Non-Uniform Rational B-Splines Representation versus Polynomial Surface Description in a Freeform Three-Mirror Anastigmat. *Photonics* **2024**, *11*, 875. <https://doi.org/10.3390/photonics11090875>

Received: 19 July 2024

Revised: 30 August 2024

Accepted: 6 September 2024

Published: 18 September 2024



**Copyright:** © 2024 by the authors. Licensee MDPI, Basel, Switzerland. This article is an open access article distributed under the terms and conditions of the Creative Commons Attribution (CC BY) license (<https://creativecommons.org/licenses/by/4.0/>).

## 1. Introduction

Optical design consists of finding the right sets of parameters to allow an instrument to perform a specific function. These parameters are determined by finding relevant combinations of optical surfaces, reflective or refractive, and the fine-tuning of the shapes, positions, and orientations of these surfaces using non-linear numerical optimization algorithms. The optimization of a combination of optical surfaces is usually performed using dedicated optical design software, such as Synopsys CodeV or ANSYS-ZEMAX OpticStudio (OpticStudio). An appropriate solution is typically a compromise between

performance metrics, such as the modulation transfer function or geometric spot diameter, and practical constraints, such as the volume, cost, and weight.

It is becoming increasingly common to use freeform surfaces in optical design [1]. A freeform optical surface is typically defined as a non-rotationally symmetric surface that cannot be described as an off-axis section of a conicoid. These surfaces are more effective than previous off-axis solutions in many of the aforementioned metrics due to an increased number of degrees of freedom (DOFs) [2]. However, these added DOFs can be a real impediment for the optical designer in finding an optimal system as they can induce saddle points in the merit function topology. A saddle point is characterized by having a gradient equal to zero in all directions but is not a local extremum of a function. In particular, this impacts local optimization algorithms, which rely on gradient descent to find the local minimum of a merit function. New design methods are being developed to address these added challenges and can be sorted into methods for the generation of a starting point, the development of optimizers, and the choice of a surface representation. This article aims to provide some insights on the latter.

Starting point generation methods commonly rely on solving partial differential equations typically based on the Fermat path principle [3]. These equations can be solved close to the on-axis chief ray (sometimes called paraxial ray) such as in the First-Time-Right (FTR) method [4] or extended to the construction of 3D surfaces by numerically integrating higher-order derivatives of these equations [5]. Other methods rely on the direct construction of the surfaces, such as the SMS method [6], which generalizes the Cartesian oval principle, leading to the design of monochromatic systems with a number of rigorously stigmatic field points equal to the number of surfaces. A design method based on this approach was developed by Mayeur et al. in the context of dioptric systems in the infrared region [7]. Additionally, other construction methods were developed such as iterative construction using the point-by-point method [8–10] or methods relying on artificial intelligence [11].

The methods mentioned above allow a freeform system to be designed directly; however, they are generally well corrected over one or several discrete field points, and hence they must also be optimized. The most common method relies on understanding and mathematically describing the behavior of the geometrical aberrations. This is the objective of the Nodal Aberration Theory (NAT), extended to freeform systems [12]. However, optimization algorithms still need to be used [13]. The development of evolutionary algorithms, which can bypass the problems caused by the presence of local minima and saddle points in the merit function topology, is another area of interest [14,15]. An optical design tool using the Covariance Matrix Adaptation—Evolution Strategy (CMA-ES) algorithm was developed and allows an entire landscape of solutions to be explored and to quickly converge in a single optimization step [16,17].

Finally, a significant aspect of freeform optical design is the choice of a surface representation, which has been discussed in [18–20]. The most common way to represent a freeform surface relies on describing the sag of the surface with an analytical formula using 2D polynomials. Several bases are typically used, and an extensive summary can be found in [21], while Chrisp [22] pioneered the use of Non-Uniform Rational Basis Splines (NURBS) in optical design of imaging systems. NURBS are well-suited for representing freeform surfaces compared to polynomials because they exhibit interesting mathematical properties, such as local control of the surface shape. They do not require any prior knowledge of the surface and are already commonly used in Computer-Assisted Design (CAD) software, which is interesting from an opto-mechanical standpoint. NURBS use a grid of weighted control points to impact a surface over a limited area. This contrasts with polynomial surfaces, where every polynomial term affects the entire surface. The requirements to optimize a NURBS system differ from those in commercial optical design software, mainly due to the high number of degrees of freedom. For that reason, commercial design software empirically shows poor performances in optimizing NURBS, and the use of custom-made software is required. Fast Accurate NURBS Optimization (FANO) [23] software utilizes

parallelized ray tracing to trace a large number of rays (over 50,000). Moreover, FANO uses about 4000 grid points to sample the surfaces. Given the large number of rays being traced, FANO was designed to perform fast ray tracing and to communicate with other programs, such as CodeV, FRED, and DIFFSYS. In this study, we used the Freeform Optics Raytracer with Manufacturable Imaging Design cApaBiLitiEs (FORMIDABLE) software [24], under ESCL license [25] and available at [26], to optimize NURBS surfaces. This software uses differential ray tracing (described in the following section), which allows the optimization of complex surfaces such as NURBS with a number of rays similar to those used in commercial optical design software. This makes FORMIDABLE much less resource-heavy software than FANO.

## 2. Materials and Methods

This paper compares how optimizing systems using NURBS surfaces perform against polynomial descriptions. NURBS surfaces are optimized with FORMIDABLE, while polynomial surfaces are optimized with OpticStudio, a commercial optical design software. The FORMIDABLE software capabilities are detailed in [24]. We list some of the most interesting features of the software:

- Differential ray tracing, which simultaneously computes the rays and their derivatives when tracing them. A ray is defined as a line perpendicular to a wavefront and can be represented by a point and a normalized direction vector. Rays being reflected and refracted by the optical surfaces form the ray path, which does not necessarily have an explicit analytical expression. In FORMIDABLE, differential ray tracing is implemented in two ways: using implicit differentiation applied to the calculation of the intersection between a ray and a surface or using the differentiation of the offense to the Fermat path principle [24].
- Merit function differentiation, using Automatic Differentiation (AD) [27].
- Projected apertures, which can be used to define an aperture on NURBS surfaces, whereas optical design software usually only consider surfaces that are defined with a sag. The projected aperture is defined on a plane in front of the NURBS that is projected on it.
- Ray aiming, which allows the aperture stop to be placed at any desired location. It is implemented using black-box algorithms in commercial optical design software and might not be considered in FANO. FORMIDABLE performs ray aiming using an algorithm in three steps. The algorithm finds the on-axis chief ray (OAR) and computes the physical pupil of the system, which then allows the computation of a raymap through backward propagation. These points intersect the pupil at the correct position but do not originate from the correct points in the field of view (FOV). Ray tracing from the correct field points is achieved through direct propagation and uses the rays in the raymap as guesses to find the ray that intersects the pupil at the correct location. Then, non-physical rays are eliminated.
- Use of external optimizers. Tests have shown that the Levenberg–Marquart algorithm performed well on optical systems. We used the open source implementation from the SciPy library [28].

For reference, OpticStudio documentation can be found in the OpticStudio User Manual.

The starting point for the off-axis three-mirror anastigmat (TMA) presented here was first designed in OpticStudio with spherical surfaces. It is illustrated in Figure 1, and its characteristics are presented in Table 1. As can be expected from the use of spherical mirrors in fast, wide, FOV, off-axis telescopes, the aberrations need to be corrected.

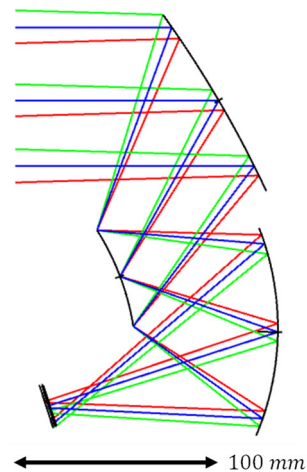


**Figure 1.** Optical layout of the starting point. Three FOVs are represented:  $+Y_{max}$  (red),  $0^\circ$  (blue), and  $-Y_{max}$  (green).

**Table 1.** Paraxial parameters of the studied system.

Parameter	TMA
Focal length [mm]	100
Field of view [ $^\circ \times ^\circ$ ]	$4.4 \times 3.3$
Stop location	$M_2$
Aperture semi-diameter [mm]	22.235
$F_\#$	1.5

We used this starting point in both FORMIDABLE and OpticStudio. To ensure a fair comparison between the two software tools, the merit functions (MFs) were defined using the same parameters and arranged to be as similar as possible. However, it was not possible to strictly define the same MFs. The MF is defined using five main parameters, which are explained below:

- Pupil sampling corresponds to the number and repartition of rays used to sample the pupil of the system. We used rectangular array sampling with  $21 \times 21$  points for FORMIDABLE, which requires an odd value to sample the center of the pupil. The closest attainable values with OpticStudio were either  $20 \times 20$  or  $22 \times 22$ . Both were tested, and the values yielding the best optimization results were kept ( $20 \times 20$ ). The difference between both these settings was marginal.
- Field sampling corresponds to the number and the repartition of point sources in the FOV. We used rectangular array sampling with  $5 \times 5$  points.
- The optimization criterion corresponds to the OpticStudio Default Merit Function Start (DMFS) operand, which can be set in the Optimization Wizard. Standard criteria include spot the radius or the wavefront error. We chose to optimize over the root mean square (RMS) spot radius. In FORMIDABLE, the equivalent setting is called “TransverseAberration”.

We also chose to use two types of constraint operands.

- The first one allows the focal length of the system to be maintained. In OpticStudio, the EFFL operand can be used for centered optical systems. However, it cannot be used for off-axis systems, and such an operand was not implemented in FORMIDABLE. We thus minimized the distance between the position of the real centroids and those given by the following equation for eight points at the edges of the FOV and an additional one at the center of the FOV:

$$y' = f' \tan(\theta). \tag{1}$$

In this equation,  $y'$  is the centroid position on the image plane of a system with a focal length  $f'$  of a point source at an angle  $\theta$ .

In OpticStudio, this can be achieved using the CENX and CENY operands and simple mathematical operations. In FORMIDABLE, we used the “centroid\_goals” parameter within the “TransverseAberration” operand.

- The second operand allows the ray clearance of the system to be defined in order to avoid vignetting. The implementation of the RayClearance operand in FORMIDABLE is based on the JMRCC operand in CodeV [29]. The geometry of the NURBS system is frozen by guaranteeing that the ray clearances keep their respective values at the beginning of the optimization. A similar implementation was carried out in OpticStudio using the RAGY, RAGX, RAGB, and RAGC operands as well as simple mathematical operations. In the systems optimized with OpticStudio, the surfaces’ positions and orientations were not used as variables.

The interested reader may refer to FORMIDABLE’s SpaceCodev repository for more details on the implementation of the TMA and the merit function in FORMIDABLE [26]. The parameters used, corresponding operands, and settings are summarized in Table 2 for both FORMIDABLE and OpticStudio.

**Table 2.** Merit function parameters and their respective implementations in FORMIDABLE and OpticStudio.

MF Parameter	FORMIDABLE	OpticStudio
Pupil Sampling Type	Rectangular Array	Rectangular Array
Pupil Sampling Value	21 × 21	20 × 20
Field Sampling Type	Rectangular Array	Rectangular Array
Field Sampling Value	5 × 5	5 × 5
Optimization Criterion	TransverseAberration	Spot (TRCX/TRCY)
Focal Length Operands	centroid_goals	CENX/CENY
Ray Clearance Operands	RayClearance	RAGY/RAGX/RAGB/RAGC

The optimization was carried out using either OpticStudio’s local optimization tool or SciPy’s implementation of the Levenberg–Marquardt algorithm for optimizations in FORMIDABLE. The optimization was performed over the surface shape while maintaining the surface position and orientation fixed with respect to the starting point. When using OpticStudio, we chose to work with XY polynomials (also called “Extended Polynomials” in OpticStudio). We made this choice arbitrarily on the basis that the choice of a polynomial surface description was not of significant importance compared to imaging quality criteria and parameters, as suggested by several studies [19,30]. The surface sag can thus be described by the following:

$$z(x, y) = \frac{(x^2 + y^2)c}{1 + \sqrt{1 - c^2(x^2 + y^2)}} + \sum_{i=0}^N \sum_{j=0}^{N-i} a_{ij} x^i y^j. \tag{2}$$

In this equation,  $x, y$  represent the local pupil coordinates in a cartesian coordinate system,  $c$  is the surface curvature, and  $\{a_{ij}\}_{i,j \in \llbracket 1, N \rrbracket^2}$  are weight coefficients assigned to the XY polynomial indexed by  $i, j$ .

Polynomial surfaces were initially described up to order 5 ( $N = 5$ ) and increased to order 7 ( $N = 7$ ) to compare lower- and higher-order surfaces with NURBS. As the systems share a planar symmetry along the YZ plane, only the radius of the curvature and polynomial coefficients with even powers of X were optimized. In addition, the term



$X^2 + Y^2$  needs to be kept to zero as it is redundant with the radius of the curvature. The term  $X^2 - Y^2$  is not redundant and must be kept. Thus, we set the  $X^2$  coefficient to zero as well.

In FORMIDABLE, NURBS surfaces are defined using a parametric form that depends on two parameters  $u$  and  $v$  as well as a set of control points  $P$ :

$$S(u, v) = \frac{\sum_{i=0}^m \sum_{j=0}^n N_{i,p}(u) N_{j,q}(v) w_{i,j} P_{i,j}}{\sum_{i=0}^m \sum_{j=0}^n N_{i,p}(u) N_{j,q}(v) w_{i,j}}. \tag{3}$$

$N_{i,j}$  are B-Spline basis functions defined recursively using the Cox–de Boor recurrence relation;  $\{w_{i,j}\}$  are the weights assigned to each control point; and  $(p, q)$  are the degrees of the NURBS along  $u$  and  $v$ , respectively [31]. In this work, NURBS are described using 3rd-order splines with a grid of  $6 \times 6$  control points. For a fixed number of control points, the use of higher-order splines reduces the NURBS locality. Therefore, using 3rd-order splines is a usual default setting when representing freeform surfaces with NURBS as a higher order might generate more extreme local curvatures [32]. This provides a high locality without drastically increasing the number of control points. The number of control points was chosen as a compromise between the number of degrees of freedom and computational speed. For the NURBS system, each control point has 4 degrees of freedom (the position of the control point in a three-dimensional space and a weight), resulting in 144 degrees of freedom per surface. As a result, there are 432 degrees of freedom. Additionally, FORMIDABLE considers, by default, a symmetric transformation that applies the same value along a chosen symmetry axis. This allows us to divide the number of effective degrees of freedom by 2. The total number of degrees of freedom used in each optimization case is given in Table 3. It is apparent that NURBS require many more degrees of freedom than polynomial descriptions (4 to 7 times more in this case) which justifies the use of differential ray tracing. This allows us to directly compute the Jacobian matrix of the optimization problem and feed it directly to the optimizer instead of numerically computing it, which saves time and computational resources. In this study, we restricted ourselves to the use of symmetric NURBS, but it is also possible to consider non-symmetric NURBS, in which case the number of degrees of freedom is twice as large.

**Table 3.** Number of degrees of freedom used in each optimization case.

Optimization Case	NURBS	XY5	XY7
Number of Degrees of Freedom	216	30	54

We ran several optimizations iterating over various cycle numbers, ranging from 5 to 200. We added an optimization with an “Automatic” stop condition for XY5 and XY7 systems. The duration of each optimization cycle was also evaluated.

To compare our results, we used the RMS field map, which corresponds to the RMS radius of the spot diagram as a function of the FOV. More specifically, we used the average value of this RMS field map ( $\langle RMS \rangle$ ) as the major figure of merit for our comparison, and we also plotted the standard deviation across the FOV with respect to  $\langle RMS \rangle$  as well as the minimum and maximum values. The diffraction limit in the long-wave infrared region (LWIR, 8  $\mu\text{m}$ ) is plotted as well, along with the minimum wavelength, which results in a diffraction-limited system for each system. We also used the total optimization duration as a comparison criterion. Then, we compared one of the results obtained in each of the optimization cases. We performed a full RMS field map comparison along with a comparison of the mirror shapes to assess differences in manufacturability. All the results are provided in the following section.

### 3. Results

This section is divided in two main subsections. In the first subsection, we present the results obtained from the systematic comparative study. Then, we zoom in on a single iteration of each system to make a detailed comparison.

#### 3.1. Systematic Approach

This study aims to highlight the impact of surface representation on optical imaging quality post-optimization and computing time.

We first compared the imaging performance of the NURBS system optimized with FORMIDABLE against those optimized in OpticStudio and described by XY polynomials. In Figure 2, the RMS spot radii are averaged over the FOV and represented in a full line for each optimization case as a function of the number of iteration cycles. The standard deviation of the RMS spot radii variation across the FOV is represented by the colored ribbon, which estimates the uniformity over the whole FOV. Finally, the vertical error bars represent the minimum and maximum values. We chose a step of 10 iteration cycles, except between 0 and 20 cycles, where a step of 5 cycles was chosen to determine how the optimization behaves before reaching a threshold.

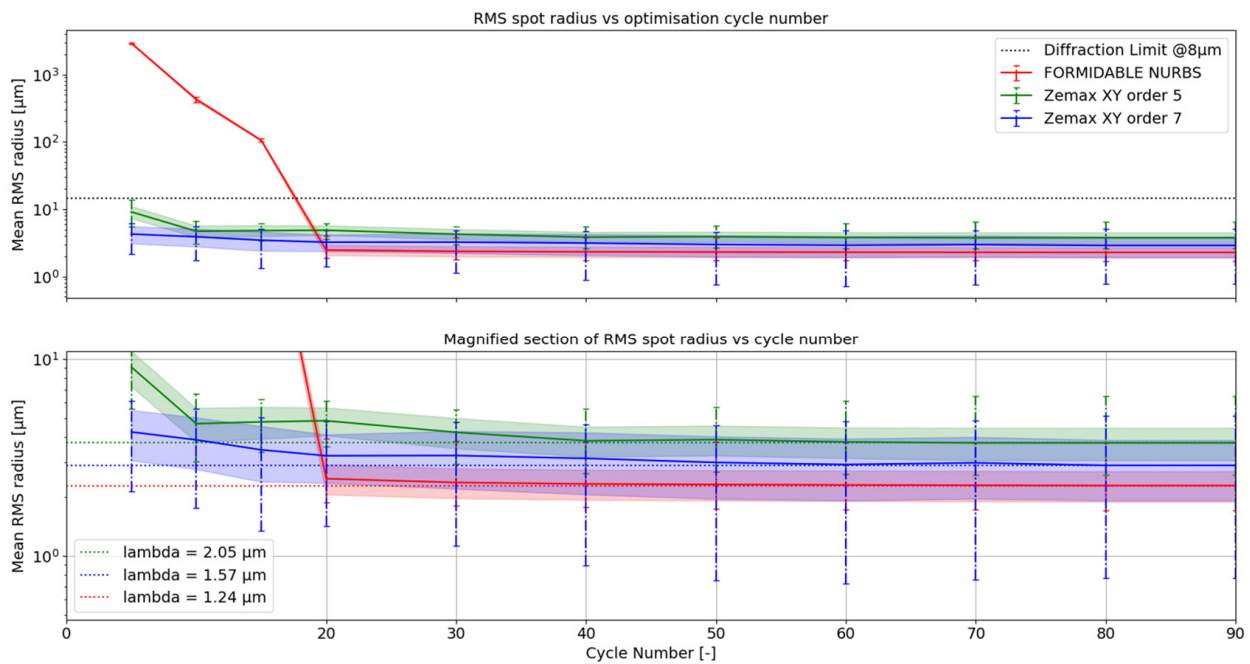


**Figure 2.** Averaged RMS spot radii across the FOV as a function of the number of optimization cycles for a TMA system. For each system, the colored ribbon represents the standard deviation of the RMS radius distribution across the FOV, and the error bars represent the minimum and maximum RMS radii across the FOV. The Airy spot radius is 14.4 µm at a 8 µm wavelength and is represented with a black dotted line. The colored dotted lines correspond to the Airy spot radius at different wavelengths in the short-wave infrared region. They are the wavelengths that correspond to a diffraction-limited system using the average field spot radius.

As seen on the top panel, each system can be optimized well below the diffraction limit (in the LWIR, at 8 µm) after a few optimization cycles. However, it takes a few more optimization cycles with FORMIDABLE to achieve the same correction level than OpticStudio. After 40 cycles, a plateau is reached, and subsequent improvement in optical quality is marginal. This behavior is maintained through the maximum number of cycles used (200) and with OpticStudio systems even after pushing the local optimization in “Automatic” mode. For clarity of representation, we only plotted up to 90 cycles on this graph. The bottom panel is a magnified view around the imaging performance plateau



to better showcase the differences between each system. The dotted lines represent the asymptotic average RMS spot radius and can be linked to the Airy radius of a diffraction-limited system at a wavelength indicated in the legend of the bottom panel. It appears that the NURBS TMA provides an image quality as good as those of the polynomial TMAs in the LWIR, albeit with a smaller deviation in the spot radius field distribution. The image uniformity is also much better in the NURBS TMA, which suggests a better opto-mechanical tolerance as shown in Kopon's article [33]. Upon later releases of the feature, more advanced studies on the tolerancing of NURBS systems in FORMIDABLE will be performed. For shorter wavelengths, however, these results suggest that NURBS allow diffraction-limited performance to be reached at lower wavelengths than polynomial systems. In this case, taking the average RMS spot radius as a reference, the NURBS TMA can achieve diffraction-limited performance down to  $1.24\ \mu\text{m}$ , while the polynomial TMAs may only be diffraction-limited to  $1.57\ \mu\text{m}$  and  $2.05\ \mu\text{m}$  at orders 7 and 5, respectively. As a result, combined with the spot radii uniformity in the FOV, a NURBS TMA might be more interesting for multispectral applications. The main challenge is to have a small enough aperture ratio to use an uncooled microbolometer while maintaining an image quality sufficient to image other spectral bands.

We also compared the time required to perform each optimization, which is represented in Figure 3. The cumulative optimization time is represented as a function of the number of optimization cycles. We noticed that there are no significant differences between the optimization of the NURBS TMA and a polynomial TMA at order 7. However, the polynomial TMA at order 5 was much faster to optimize with a similar machine workload. For reference, all the optimizations were performed with an Intel® Core™ i7-1265U CPU @4.8 GHz with 12 threads and 16 GB RAM. Optimizations with FORMIDABLE and OpticStudio were run separately and in the same operation conditions.

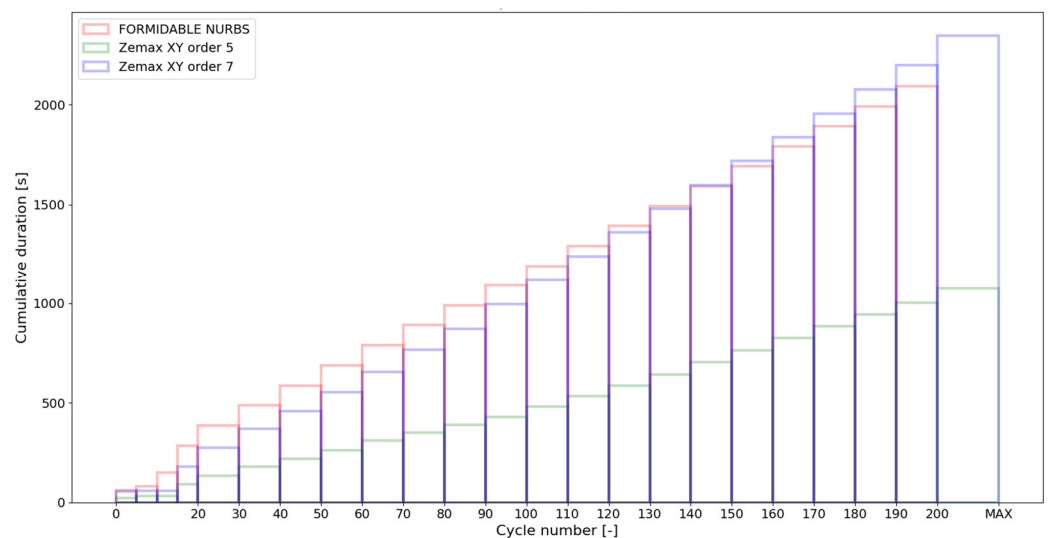


**Figure 3.** Cumulative optimization time as a function of the number of optimization cycles.

### 3.2. Detailed Comparison between NURBS and Polynomial TMA

In addition to the previous analyses, we compare an iteration of the NURBS TMA and polynomial TMA at orders 5 and 7. We chose to compare the systems optimized with 80 cycles since according to Figures 2 and 3 they are a good compromise between the optimally achieved imaging quality and optimization duration. The optical imaging quality comparison was made using the RMS field maps. These were plotted using FORMIDABLE's algorithm to compare each system accurately. Figure 4 represents the RMS field map of each of these systems on the same scale. The NURBS TMA is on the left, and the polynomial TMAs are on the right. As suggested from Figure 2, the NURBS TMA displays a much more uniform RMS field map compared to the polynomial one, which

is especially true when comparing the NURBS and the XY7 systems. The XY5 exhibits a smoother RMS field map than the XY7 system, but with significantly larger spot radii than the NURBS TMA. Even if the XY7 TMA’s average RMS spot radius is lower than the XY5 TMA’s, the RMS spot radius distribution across the FOV is no longer uniform. It may be explained because higher polynomial orders improve the average imaging quality, to the detriment of uniformity. Additionally, while the RMS field map of the XY5 TMA is also uniform, the NURBS TMA exhibits lower RMS spot radii.

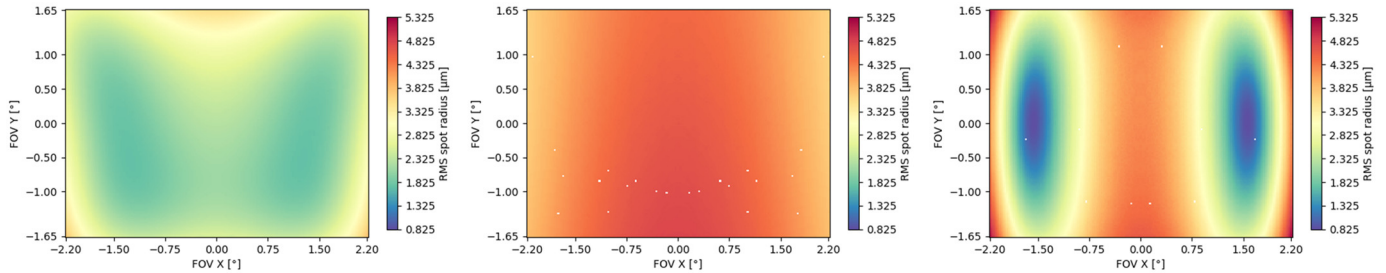


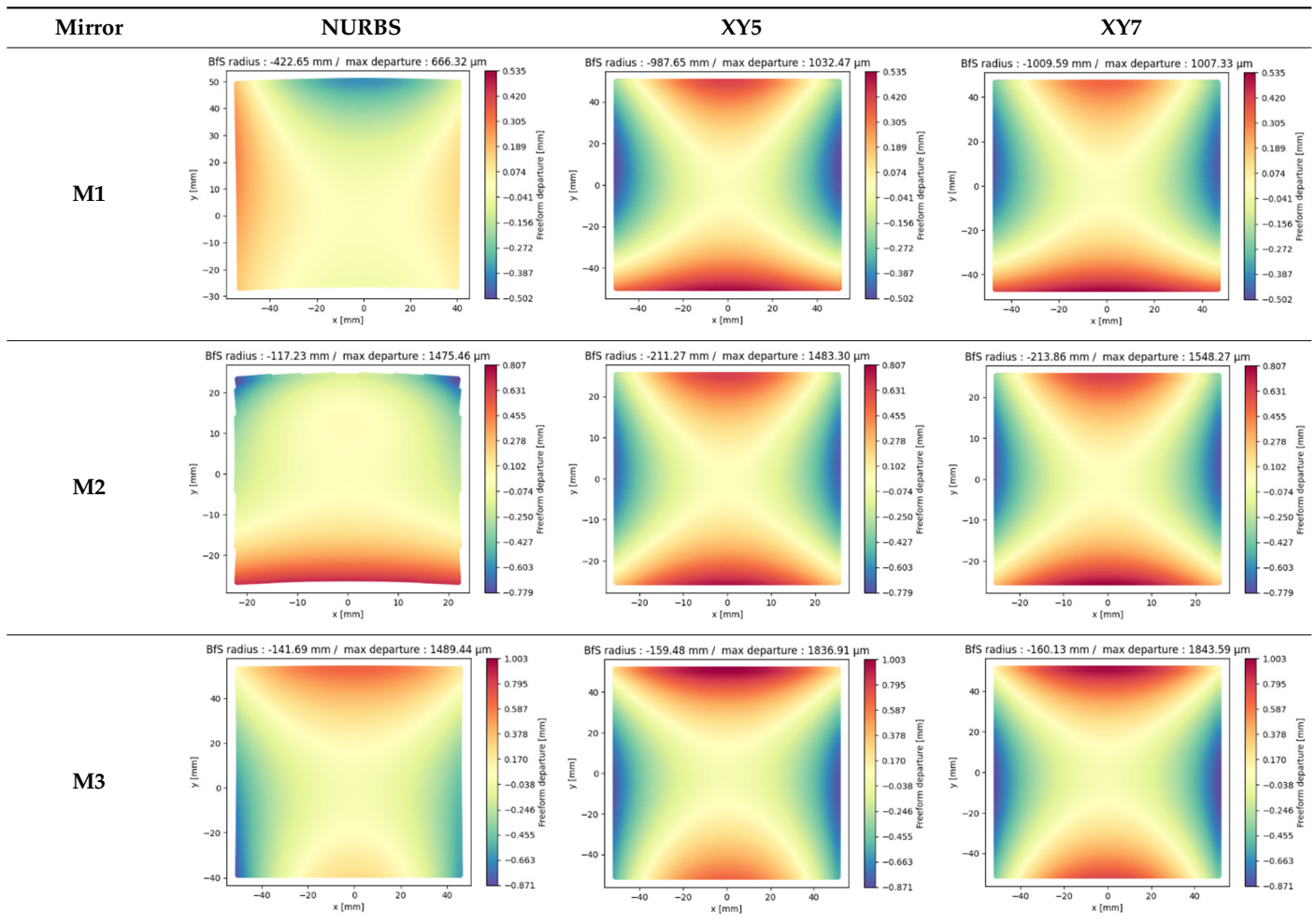
**Figure 4.** RMS field maps of the NURBS TMA (left), XY5 TMA (center), and the XY7 TMA (right). The scale is common for each map.

Finally, we compared the shape of the freeform mirrors. We plotted the deviation from the best-fit sphere of each mirror computed on its clear aperture only. The results are displayed in Table 5, which illustrates the freeform departure maps of each mirror, and in Table 4, which indicates the radius of the curvature of the best-fit sphere (“BfS radius”) and the RMS freeform departure of each surface from that sphere. The maximum freeform departures of  $M_1$  in the NURBS TMA are smaller than those of the XY5 and XY7 ones by about 50%. Similarly, the peak-to-valley variation in freeform departures for the NURBS  $M_3$  is about 25% smaller than those of its XY counterparts. The secondary mirror ( $M_2$ ) shares similar freeform departures in each case. Furthermore, the average RMS freeform departure is smaller for the NURBS TMA. This indicates that overall, the mirrors of the NURBS TMA are slightly easier to manufacture than those of the XY5 or XY7 ones. We can also notice that the freeform shapes of the mirrors in both XY5 and XY7 cases are similar, along with the RMS freeform departures. In addition, the NURBS mirrors are less symmetrical than the polynomial ones. This indicates that NURBS can be used to achieve mirror shapes that freeform polynomial surfaces would not be able to achieve unless significantly increasing the polynomial order.

**Table 4.** Best-fit spheres and RMS freeform departures.

BfS Radius of Curvature (mm)	NURBS	XY5	XY7
<b>M1</b>	−422.65	−987.65	−1014.58
<b>M2</b>	−117.23	−211.27	−213.86
<b>M3</b>	−141.69	−159.48	−160.13
RMS Freeform Deviation (μm)	NURBS	XY5	XY7
<b>M1</b>	116.5	217.8	242.2
<b>M2</b>	237.7	308.0	320.0
<b>M3</b>	264.9	367.1	375.6
<b>Average</b>	206.4	297.6	312.6

Table 5. Freeform departure maps.



#### 4. Discussion

In this article, we compared the performance of a NURBS TMA optimized with FORMIDABLE versus polynomial TMAs designed with OpticStudio using XY polynomials. The design strategy and merit function, as well as optimization duration, were as similar as possible in each case to ensure that comparisons could be made. We designed NURBS surfaces with a symmetric distribution of the control points to reduce the number of degrees of freedom. However, using every control point as a variable could result in less conventional surface shapes and may also be investigated. The results achieved in this study show that a NURBS TMA optimized with FORMIDABLE does not take longer to optimize than a polynomial TMA optimized with OpticStudio. In addition, the NURBS TMA exhibits slightly better average RMS spot radii and improves the uniformity of the spot radii across the FOV compared to its polynomial counterparts. As a result, the NURBS TMA can be diffraction-limited over a larger spectral range and seems to be a slightly better alternative for multispectral applications using a single optical path for each spectral channel. In addition, the better spot uniformity may indicate a better system behavior in response to opto-mechanical errors. A better spot uniformity reduces the need to compromise between imaging performance at the edge or at the center of the FOV, which may allow the depth of field to be increased. This result is in accordance with Kopon et al.'s study, which compared a NURBS freeform TMA to conventional aspheric and Zernike freeform telescopes with similar designs and concluded that the NURBS TMA was as sensitive to alignment errors and half as sensitive to thermal changes compared to the conventional designs [33]. The results we achieved suggest that the third-degree NURBS

can lead to performances better than or similar to higher-order polynomials and better uniformity without increasing the RMS freeform departures of the mirrors. Thus, in the context of reflective imaging systems for nanosatellites, NURBS surfaces allow a more uniform distribution of the RMS spot radii in the FOV to be achieved without inducing significantly more complex surface shapes compared to high-order XY polynomials. They may also benefit multispectral applications using a single optical path for each spectral channel.

Additionally, we can compare our results to those of Chrisp, who used FANO to optimize a freeform TMA with NURBS surfaces and compared it to an aspherical and a freeform TMA using XY polynomials up to order 10 [34]. Compared to our study, Chrisp also used the odd powers of  $X$  as variables. In addition, in FANO, the NURBS freeform design is optimized with about 4000 control points ( $37 \times 37$  for  $M_1$ ,  $29 \times 29$  for  $M_2$  and  $41 \times 41$  for  $M_3$ ). Due to the high number of control points, FANO also uses parallelized ray tracing to trace a large number of rays (over 50,000). Chrisp's results indicate significantly better image correction with the NURBS TMA than with aspheres or XY polynomials, while the improvement we found is smaller. This could be partially due to the fact that, unlike in our study, Chrisp did not freeze the surfaces' positions or orientations, and he used significantly more control points. The spot radii uniformity also seems better with NURBS. However, the TMA optimized with FANO exhibits significantly larger freeform departures compared to the polynomial TMA (twice as large on average and 33 times larger for  $M_2$ ). Meanwhile, with FORMIDABLE, we were able to maintain the RMS freeform departures at a similar level or better than with polynomial TMAs. Both studies seem to indicate that NURBS make interesting surface descriptors for freeform TMAs. However, some differences between FORMIDABLE and FANO are worth mentioning. Compared to FANO, which uses many control points (about 4000) and rays and uses parallelized ray tracing to increase the optimization speed, FORMIDABLE uses differential ray tracing in addition to raytracing parallelization in the merit operands and is able to achieve satisfying results with far fewer variables. In our study, we used grids of  $6 \times 6$  control points for the NURBS surfaces and about 11,000 rays ( $21 \times 21$  rays to sample the pupil for each of the 25 field points). This is 5 times fewer rays, and about 36 times fewer control points. In addition, although the optimization duration is not indicated in Chrisp's article, we achieved optimization times of the same order as OpticStudio for a seventh-order XY polynomial TMA.

## 5. Conclusions

In this study, we optimized freeform TMAs with NURBS surfaces using FORMIDABLE, an optical design library with differential ray tracing capabilities. We then compared the RMS spot radii obtained against freeform TMAs designed using OpticStudio with XY polynomials up to orders 5 and 7, respectively. The results show that the NURBS TMA exhibits a better uniformity in the distribution of the spot radii across the FOV, along with slightly better imaging performance on average. This is especially interesting for multispectral applications. Indeed, with a more uniform RMS field map, the imaging performance is not impacted by a poorer image quality in some areas of the FOV. Furthermore, the RMS freeform departure of the mirrors is not larger for the NURBS TMA than for the polynomial ones, indicating that both could be manufactured with similar methods.

Finally, we discussed the results obtained with FORMIDABLE against results found with FANO, another optical design library for optimizing NURBS surfaces. We report that FORMIDABLE is able to achieve satisfying results using fewer computational resources due to the implementation of differential ray tracing. Differential ray tracing can be used to trace a number of rays, similar to those used in OpticStudio, and with significantly fewer control points than FANO uses. The duration of the optimization with FORMIDABLE is similar to that achieved with OpticStudio. We have determined that NURBSs could be an interesting surface representation. A perspective to improve FORMIDABLE would be additional performance figures of merit such as the modulation transfer function and



manufacturability figures of merit, such as orthogonal slopes, as well as tolerancing of NURBS systems. Our results suggest that NURBS surfaces do not introduce significant manufacturing difficulties. In the future, it could be interesting to further study NURBS manufacturability and alignment tolerancing.

**Author Contributions:** Conceptualization, C.F. and G.D.; methodology, C.F., G.D. and S.B.; software, J.-B.V. and S.B.; validation, C.F., G.D., A.F. and T.L.; formal analysis, C.F.; investigation, C.F.; resources, C.F. and G.D.; data curation, F.K., C.B., T.A. and A.H.; writing—original draft preparation, C.F.; writing—review and editing, C.F., A.F., G.D., T.L. and S.B.; visualization, C.F.; supervision, T.L. (director), G.D. (co-director), A.F., C.B., T.A., A.H. and J.-B.V.; project administration, F.K., G.D., P.J., S.B. and J.-B.V. All authors have read and agreed to the published version of the manuscript.

**Funding:** FORMIDABLE development was funded by the European Space Agency under contract 4000136450/21/NL/AR. Clément Freslier’s doctoral scholarship has been funded by the European Space Agency under contract No. 4000137420/22/NL/GLC/my.

**Institutional Review Board Statement:** Not applicable.

**Informed Consent Statement:** Not applicable.

**Data Availability Statement:** FORMIDABLE source code is available at <https://gitlab.space-codev.org/formidable/formidable> (accessed on 19 July 2024). Raw material and results can be found at [https://gitlab.space-codev.org/formidable/formidable\\_package/-/tree/main/articles\\_materials/TMA\\_MDPI\\_ComparativeNURBS?ref\\_type=heads](https://gitlab.space-codev.org/formidable/formidable_package/-/tree/main/articles_materials/TMA_MDPI_ComparativeNURBS?ref_type=heads) (accessed on 19 July 2024).

**Acknowledgments:** We kindly acknowledge Louis Duveau for providing the base material for the TMA used in this work and Mathieu Ehrhart for the insightful discussions.

**Conflicts of Interest:** Author J.-B.V. was employed by the company Constellr. The remaining authors declare that the research was conducted in the absence of any commercial or financial relationships that could be construed as a potential conflict of interest.

## References

1. Rolland, J.P.; Davies, M.A.; Suleski, T.J.; Evans, C.; Bauer, A.; Lambropoulos, J.C.; Falaggis, K. Freeform Optics for Imaging. *Optica* **2021**, *8*, 161. [CrossRef]
2. Schiesser, E.M.; Bauer, A.; Rolland, J.P. Effect of Freeform Surfaces on the Volume and Performance of Unobscured Three Mirror Imagers in Comparison with Off-Axis Rotationally Symmetric Polynomials. *Opt. Express* **2019**, *27*, 21750–21765. [CrossRef] [PubMed]
3. González-Acuña, R.G. Design of a Pair of Aplanatic Mirrors. *Appl. Opt.* **2022**, *61*, 1982–1986. [CrossRef] [PubMed]
4. Duerr, F.; Thienpont, H. “First Time Right”—Calculating Imaging Systems from Scratch-INVITED. *EPJ Web Conf.* **2021**, *255*, 02001. [CrossRef]
5. Volatier, J.-B.; Druart, G. Differential Method for Freeform Optics Applied to Two-Mirror off-Axis Telescope Design. *Opt. Lett.* **2019**, *44*, 1174–1177. [CrossRef] [PubMed]
6. Benitez, P.; Minano, J.C.; Blen, J.; Mohedano, R.; Chaves, J.; Dross, O.; Hernandez, M.; Alvarez, J.L.; Falicoff, W. SMS Design Method in 3D Geometry: Examples and Applications. *Nonimaging Optics: Maximum Efficiency Light Transfer VII*; SPIE: San Francisco, Philippines, 2004; Volume 5185, pp. 18–29.
7. Mayeur, T.; Volatier, J.-B.; Druart, G.; Cau, F.; Tartas, E.; Durand, A. Automatic Method of Exploring the Landscape of Freeform Dioptic Optical Problems, Working in the Infrared Region. *Optics* **2023**, *4*, 482–499. [CrossRef]
8. Yang, S.; Hu, D.; Wang, A. Point-by-Point Fabrication and Characterization of Sapphire Fiber Bragg Gratings. *Opt. Lett.* **2017**, *42*, 4219–4222. [CrossRef] [PubMed]
9. Yang, T.; Zhu, J.; Wu, X.; Jin, G. Direct Design of Freeform Surfaces and Freeform Imaging Systems with a Point-by-Point Three-Dimensional Construction-Iteration Method. *Opt. Express* **2015**, *23*, 10233–10246. [CrossRef] [PubMed]
10. Zhang, X.-Y.; Yu, Y.-S.; Chen, C.; Zhu, C.-C.; Yang, R.; Liu, Z.-J.; Liang, J.-F.; Chen, Q.-D.; Sun, H.-B. Point-by-Point Dip Coated Long-Period Gratings in Microfibers. *IEEE Photonics Technol. Lett.* **2014**, *26*, 2503–2506. [CrossRef]
11. Mao, B.; Yang, T.; Xu, H.; Chen, W.; Cheng, D.; Wang, Y. FreeformNet: Fast and Automatic Generation of Multiple-Solution Freeform Imaging Systems Enabled by Deep Learning. *Photon. Res.* **2023**, *11*, 1408–1422. [CrossRef]
12. Thompson, K.P.; Fuerschbach, K.; Schmid, T.; Rolland, J.P. *Using Nodal Aberration Theory to Understand the Aberrations of Multiple Unobscured Three Mirror Anastigmatic (TMA) Telescopes*; Sasián, J., Youngworth, R.N., Eds.; SPIE: San Diego, CA, USA, 2009; p. 74330B.
13. Sasián, J. Theory of Sixth-Order Wave Aberrations. *Appl. Opt.* **2010**, *49*, D69–D95. [CrossRef] [PubMed]

14. Houllier, T.; Lépine, T. Comparing Optimization Algorithms for Conventional and Freeform Optical Design. *Opt. Express* **2019**, *27*, 18940–18957. [[CrossRef](#)] [[PubMed](#)]
15. Sahin, F.E. Open-Source Optimization Algorithms for Optical Design. *Optik* **2019**, *178*, 1016–1022. [[CrossRef](#)]
16. Nijkerk, M.D.; Gruber, J.M.; Boonacker, B. Freeform Optics Design Tool for Compact Spectrometers. In Proceedings of the International Conference on Space Optics—ICSO 2018, Chania, Greece, 9–12 October 2018; Volume 11180, pp. 780–788.
17. Héron, S.; Semet, Y.; Barrère, R.; Lee, M.-S.-L.; Loiseaux, B. Automated Design of Freeform Off-Axis Three-Mirrors-Anastigmat. Imaging Systems and Applications; Optica Publishing Group: Seattle, WA, USA, 2022; p. IW3C.2.
18. Muslimov, E.; Hugot, E.; Jahn, W.; Vives, S.; Ferrari, M.; Chambion, B.; Henry, D.; Gaschet, C. Combining Freeform Optics and Curved Detectors for Wide Field Imaging: A Polynomial Approach over Squared Aperture. *Opt. Express* **2017**, *25*, 14598–14610. [[CrossRef](#)] [[PubMed](#)]
19. Duveau, L. Freeform Mirror Designs for Aerospace Multi Spectral Band Imaging Systems. Ph.D Thesis, Université de Lyon, Lyon, France, 2022.
20. Brömel, A. *Development and Evaluation of Freeform Surface Descriptions*; Friedrich-Schiller-Universität Jena: Jena, Germany, 2018.
21. Houllier, T. Optical Imaging Systems with Freeform Surfaces: Optimization Algorithms Study and Freeform Surfaces Metrology. Ph.D Thesis, Université de Lyon, Lyon, France, 2021.
22. Chrisp, M.P. *New Freeform NURBS Imaging Design Code*. *Classical Optics 2014*; Optica Publishing Group: Koala Coast, HA, USA, 2014; p. ITh3A.7.
23. Fast Accurate NURBS Optimization (FANO)—Sc22. Available online: <https://sc22.mghpcc.org/project/fast-accurate-nurbs-optimization-fano/> (accessed on 14 June 2024).
24. Volatier, J.-B.; Beaussier, S.J.; Druart, G.; Jouglu, P.; Keller, F. Implementation of FORMIDABLE: A Generalized Differential Optical Design Library with NURBS Capabilities. *J. Eur. Opt. Soc.-Rapid Publ.* **2024**, *20*, 2. [[CrossRef](#)]
25. ESSR—License European Space Agency Community License—v2.4 Strong Copyleft (Type 1). Available online: <https://essr.esa.int/license/european-space-agency-community-license-v2-4-strong-copyleft-type-1> (accessed on 14 June 2024).
26. Formidable/Formidable GitLab. Available online: <https://gitlab.space-codev.org/formidable/formidable> (accessed on 14 June 2024).
27. Baydin, A.G.; Pearlmutter, B.A.; Radul, A.A.; Siskind, J.M. Automatic Differentiation in Machine Learning: A Survey. *arXiv* **2015**. [[CrossRef](#)]
28. Moré, J.J. The Levenberg-Marquardt Algorithm: Implementation and Theory. In *Numerical Analysis*; Watson, G.A., Ed.; Lecture Notes in Mathematics; Springer: Berlin/Heidelberg, Germany, 1978; Volume 630, pp. 105–116, ISBN 978-3-540-08538-6.
29. Rodgers, J.M. *Control of Packaging Constraints in the Optimization of Unobscured Reflective Systems*; SPIE: Los Angeles, CA, USA, 1987; p. 143.
30. Reshidko, D.; Sasian, J. Method for the Design of Nonaxially Symmetric Optical Systems Using Free-Form Surfaces. *Opt. Eng.* **2018**, *57*, 101704, Erratum in *Opt. Eng.* **2021**, *60*, 119801. [[CrossRef](#)]
31. Piegl, L.; Tiller, W. *The NURBS Book*; Springer Science & Business Media: Berlin, Germany, 2012; ISBN 3-642-59223-6.
32. Freslier, C.; Druart, G.; Fontbonne, A.; Lépine, T.; Keller, F.; Buisset, C.; Agocs, T.; Hélière, A.; Volatier, J.-B.; Beaussier, S.; et al. Optimization of a Freeform TMA with a Differential Ray Tracer with NURBS Capabilities. *Optical Design and Engineering IX*; Babington, J., Lépine, T., Gross, H., Eds.; SPIE: Strasbourg, France, 2024; p. 24.
33. Kopon, D.; Montague, J.; Primeau, B.; Krastev, P.; Cappiello, G.; Johnson, J. Sensitivity Comparison of a NURBS Freeform Telescope. *Optomechanical Engineering 2023*; SPIE: Strasbourg, France, 2023; Volume 12669, pp. 122–131.
34. Chrisp, M.P.; Primeau, B.; Echter, M.A. Imaging Freeform Optical Systems Designed with NURBS Surfaces. *Opt. Eng.* **2016**, *55*, 071208. [[CrossRef](#)]

**Disclaimer/Publisher’s Note:** The statements, opinions and data contained in all publications are solely those of the individual author(s) and contributor(s) and not of MDPI and/or the editor(s). MDPI and/or the editor(s) disclaim responsibility for any injury to people or property resulting from any ideas, methods, instructions or products referred to in the content.